Investigation of Collision Welding by High-Speed Imaging

B. Niessen*, P. Groche

Institute for Production Engineering and Forming Machines (PtU), The Technical University (TU) of Darmstadt, Germany
*Corresponding author. Email: niessen@ptu.tu-darmstadt.de

Abstract

Collision welding bases on the oblique collision of two joining partners at high relative velocities. Until today, the mechanisms of collision welding are not yet fully understood due to the variety of phenomena occurring during the collision. One of these phenomena is the cloud of particles whose influence on bond formation has been neglected concerning its stored thermal energy. For the investigation of this influence, a collision welding model test rig was used which allowed the precise adjustment of the process parameters. The process observation was implemented by an image intensifier camera to visualize the ongoing collision and the occurring process phenomena. In this manuscript the developed methodology and the results of high-speed process observation are presented. The findings confirmed previous research regarding the shape formation of the cloud of particles and the influence on bond formation. It was found that the temperature of the cloud of particles depends strongly on the collision angle. Furthermore, an accumulation of the cloud of particles during the collision process was recorded which might influence the steadiness of the welding process.

Keywords

Collision welding, High-Speed Imaging, Cloud of particles

1 Introduction

Collision welding is a solid-state welding technology that forms a metallurgical bond during the oblique collision of two joining partners, even for dissimilar metal pairings (Wang und Wang 2019). Mostly, one joining partner, called flyer, collides with a stationary so-called target under a collision angle β and at an impact velocity v_{imp} (up to 600 m/s), see **Fig. 1**. Thereby, high pressures up to several GPa and high strain rates up to 10^6 1/s occur in the collision region (Stern et al. 2014). Under these conditions, the contacting surfaces form a cumulative metal stream (called jet) which is pushed ahead the moving collision point (Cowan und Holtzman 1963; Carpenter und Wittman 1975). This jet can progress as

cumulative stream or disperse in particles. In case of a cumulative stream, its size depends on the energy input to the process (Bellmann et al. 2020; Mori et al. 2019). Additionally, due to high strain rates, brittle oxide layers and contamination layers are spalled from the surface and form a cloud of particles (CoP) which can also contain dispersed jet particles (Deribas und Zakharenko 1974). Both phenomena do not directly induce bond formation but uncover and activate the juvenile base material that forms an atomic bond due to their intimate contact (Lysak und Kuzmin 2003).
Depending on the process condition, the CoP can either be harmful or beneficial for bond formation. At small collision angles, the CoP cannot leave the closing joining gap due to air and wall friction and finally hinders the bond formation, when the collision front overtakes the CoP and re-includes it (Groche et al. 2019). Furthermore, Bellmann et al. noted that the CoP can reach high temperatures (over 5000 K) by the compression and friction in the closing joining gap (Bellmann et al. 2020). Depending on the process parameter, the thermal energy of the CoP can lead to excessive melting, especially when it is re-entrapped at small collision angles, or it enhances the plastic deformation in the collision point, when the local yield strength of the surfaces is lowered due to heating by the passing CoP (Niessen et al. 2020). Results from high-speed imaging are shown below, supporting recent findings on the important role of CoP in collision welding.

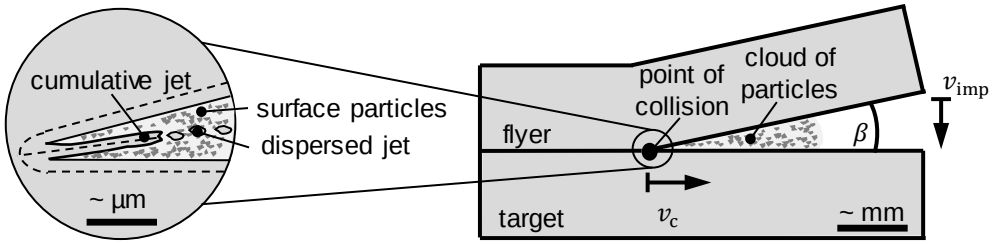

Figure 1: Schematic illustration of a collision welding process: the flyer collides with the target at the impact velocity v_{imp} and at the collision angle β (Bellmann et al. 2020; Carpenter und Wittman 1975). A cumulative jet is formed as a material flow (see detail) at the point of collision and moves ahead with the collision point velocity v_c. The formed CoP can either consist of dispersed jet particles and/or spalled oxide and contamination layers.

2 Experimental Setup

2.1 Model Test Rig

The model test rig was developed to provide adjustable and steady process parameters with a good process observability for the investigation of the collision welding phenomena. The result was a purely mechanical setup, consisting of two rotors, each driven by a synchronous motor. A welding sample (welding area: 12 mm x 12.5 mm) with an effective radius of 415 mm is mounted at one end of each rotor and accelerated to half of the desired impact velocity v_{imp} by turning the rotors at a determined rotational speed n (motor maximum: 6000 rpm), **Fig. 2** (a) & (b). The resulting maximal impact velocity is 520 m/s.

Since the rotors cannot reach the desired rotational speed within one revolution, one rotor mounted on a movable hub starts turning shifted 15 mm in the axial direction of the driving shaft. Once the desired turning speed is reached, the hub is moved by a cam gear, Fig. 2 (c). The cam gear consists of a pin and a helix groove attached to the hub. The pivoted pin is pretensioned by a spring and an electronic holding magnet in a disengaging device. When the spring is released by switching off the magnet, the pin engages in the helix groove hub, which eliminates axial offset of the hub within one resolution (positioning time < 10 ms).

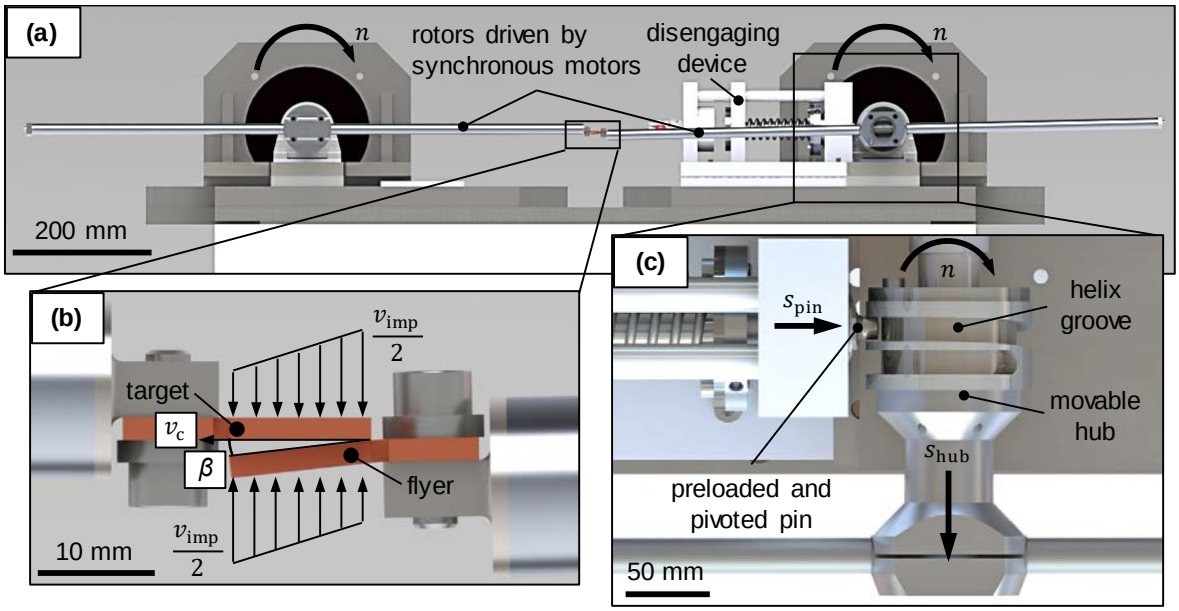

Figure 2: The main components of the model test rig (a); the samples (b) are mounted at one end of each rotor, whereby one sample (flyer) is pre-bent to determine the collision angle. A pivoted pin is preloaded in the disengaging device (c). When the pin is released, it engages with the helix groove (s_{pin}) and moves the rotor hub (s_{hub}).

2.2 Process Observation by High-Speed Imaging

A collision at these high velocities takes place in less than 10 µs and therefore requires a suitable setup for observing the collision process and the occurring phenomena. This is realized with the image intensifier camera *hsfc pro* from *PCO AG* whose optical axis is placed perpendicularly to the collision direction. The camera's exposure time can be set to less than 20 ns and allows taking up to eight images per experiment. Two lenses can be used to deliver different observation perspectives. Whereas the *Milvus 100/2.0 Makro* lens (ML) from *Zeiss* is used for a macroscopic overview of the colliding samples, the long-distance microscope (LDM) *Model K2 DistaMax* from *Infinity Photo-Optical Company* allows to observe the phenomena inside the joining gap at a high magnification up to 5 µm per pixel. An illumination laser *CAVILUX Smart* from *Cavitar* assures sufficient imaging brightness in either a transmitted or a reflected light arrangement. Since the laser emits a monochromatic red light with a wavelength of 640 nm, an optical bandpass filter can be used

to suppress the bright light flash (also known as process glare) which typically occurs during collision welding and has a broad wavelength spectrum. (Groche et al. 2017)
Due to the operating principle of the camera, it is important to provide a precise and repeatable trigger signal for the start of the collision. This is implemented by an electrical trigger. Therefore, the left rotor hub is electrically insulated from the test rig, while a voltage is applied between the test rig and the rotor by a sliding contact in the hub middle axis. When the samples collide, the electrical circuit is closed, and the measured voltage drops at a series connected high-ohmic resistor. This signal is transformed by a trigger unit in a TTL-signal for the illumination laser and an optical signal for the camera (Pabst et al. 2014).
The acquired images can be utilized in several ways. First, they deliver qualitatively more detailed information about the conditions between and around the colliding samples. Furthermore, as shown in **Fig. 3**, the collision angle β of the joining gap is measured for each image and averaged by a *MathWorks MATLAB* script using edge detection (Groche et al. 2019).

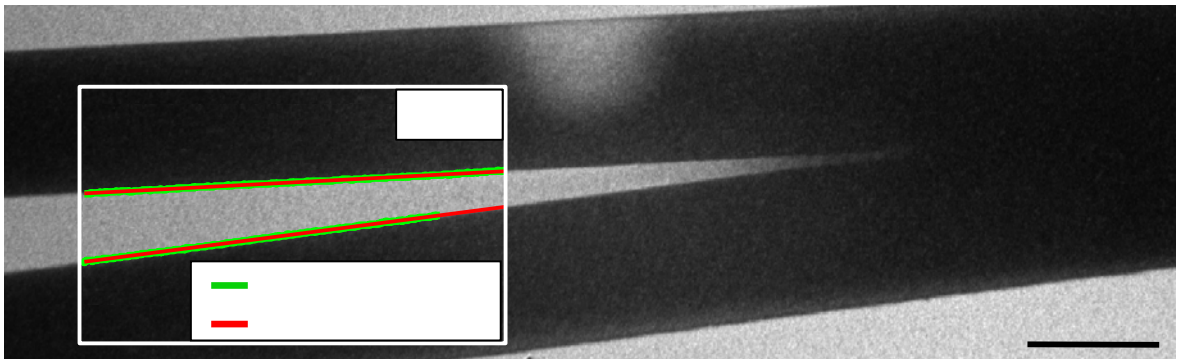

Figure 3: A MATLAB script is used to measure the collision angle at each high-speed image. The box shows the detected edge points (green). Two lines are fitted through both point clouds and the angle between them is determined.

2.3 Series of Experiments

For the following study, the investigation of high speed imaging of the process window examination for copper (Cu 99.9%, yield strength: 202 MPa) with a sheet thickness of 1 mm (see **Fig. 4**) will be deepened (Groche et al. 2019). The process parameter, i.e., impact velocity and collision angle, were varied systematically between v_{imp} = 210 m/s – 262 m/s and β = 0° – 15°. An additional series of experiments with 262 m/s was performed at four different collision angles slightly under and above the lower and upper collision angle boundary. During each experiment, four high speed images were taken in transmitted light arrangement. For the first series, the LDM was used with the bandpass filter to suppress process glare, while for the second series, the ML was mounted without bandpass filter.

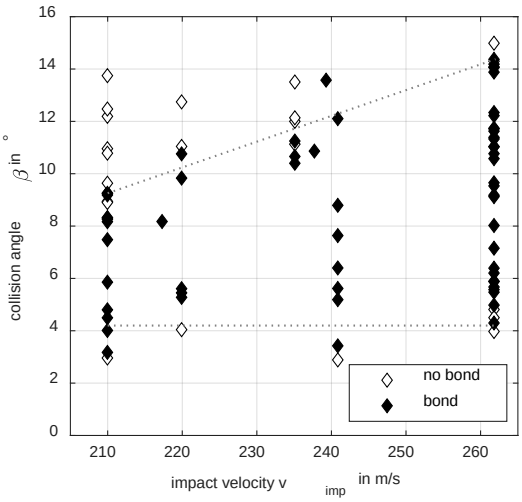

Figure 4: Process window of copper-copper joints for different impact velocities and collision angles, each marker represents one experiment. Dotted lines indicate lower and upper collision angle boundary.

3 Results and Discussion

Fig. 5 shows high speed images of two collision welding experiments: both with an impact velocity of 262 m/s at similar state of the welding process but with different collision angles. The collision angle of (a) is 5.5°, which is just over the lower boundary angle (~5.0°), whereas the collision angle of (b) is 14.1°, which is just below the upper boundary angle (~14.5°). Consequently, in both configurations a weld was achieved, but the shapes of the CoP differ significantly. As mentioned in (Groche et al. 2019), this can be attributed to the different fluid-dynamic conditions in the closing gap, which lead to a transition from a laminar to a turbulent flow with increasing flow velocity. Due to the equal impact velocity, the collision point velocity decreases at larger collision angles, which corresponds to the flow velocity. At a certain point, the disperse CoP shape transforms into a cumulative stream.

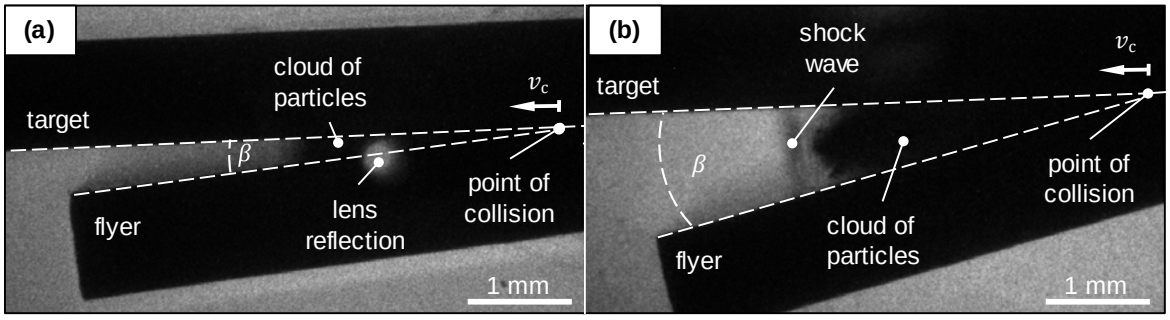

Figure 5: High speed image taken with the LDM of experiments at similar stages of the welding process with an impact velocity of 262 m/s and a collision angle of 5.5° (a) and 14.1° (b). In the smaller joining gap of (a) a dispersed CoP was visible, whereas in (b) a shaped stream is formed with dissolved single particles and shock wave in front of the CoP.

The typical shape was caused by a flow separation at the joining gap edges, where a higher velocity of the central flow and a flow deceleration at the edges resulted (Oertel und Böhle 2010). While for large collision angles like in Fig. 5 (b), a shock wave moved in front of the CoP, at small collision angles the CoP might cover or even penetrate the shock wave due to the higher flow velocity. As a result, especially at small collision angles, a high compression of the CoP and the enclosed atmospheric gases in the joining gap can be expected. This is in good agreement with Ishutkin et al., who determined the temperature of the shock compressed gas in the joining gap during explosive welding (Ishutkin et al. 1980). They also explained that the COP was responsible for the temperatures measured in the experiments being higher than those calculated for adiabatic shock compression.

As the shape of the CoP shows a dependence on the collision angle, it could be expected that there is a relation between shape and bond formation, which is also strongly influenced by the collision angle. To examine this, **Fig. 6** and **Fig. 7** compare the two cases by four high speed imaging studies for the lower and the upper collision angle boundary. For these studies, the macro lens (ML) was used to obtain more information about the CoP interaction as it leaves the gap. In former research (Bellmann et al. 2020; Bellmann et al. 2019) it is noted that the temperature in the joining gap corresponds with the brightness of the process glare. Therefore, the images were taken without bandpass filter to consider changes in its brightness. In both studies at the lower collision angle boundary, the CoP in the joining gap emitted a bright glow, which indicates a strong heating, see Fig. 6. Regarding the melted and resolidified structures at the weld interface of aluminium joints in (Niessen et al. 2020) and the determined temperature in the joining gap of several thousand Kelvin in (Bellmann et al. 2020), it can be assumed that the CoP contributed a significant part of the heat that can cause melting of the colliding surfaces also in the present configuration. On the one hand, this can be the governing bond mechanism. However, if excessive melting occurs, the contact interface may still be liquid when the contact pressure of the collision decreases, which might cause the surfaces to separate during the ongoing collision.

In both studies at the lower collision angle boundary, the amount of the CoP increased during the experiment due to the progression of the collision. At a certain process stage, the CoP started to leave the joining gap laterally, and the visible amount of laterally ejected particles was larger for series (b) with the larger collision angle. Additionally, more CoP escaped at the end of the joining gap. Hence, the non-ejected CoP might hinder the bond formation. This is in good agreement with the findings in (Niessen und Groche 2019) that the formation of the weld interface at small collision angles is only possible, where the CoP did not hinder the contact of the activated base material. Considering these two effects, the heat input of the CoP and its re-entrapment, it is not possible to distinguish which of the two factors is crucial for the prevented bond formation in the case of the series in Fig. 6 (a). It is also plausible that both effects complement each other. Nevertheless, it can be stated that the interaction of the CoP with the colliding surfaces plays a relevant role for bond formation at the lower collision angle boundary.

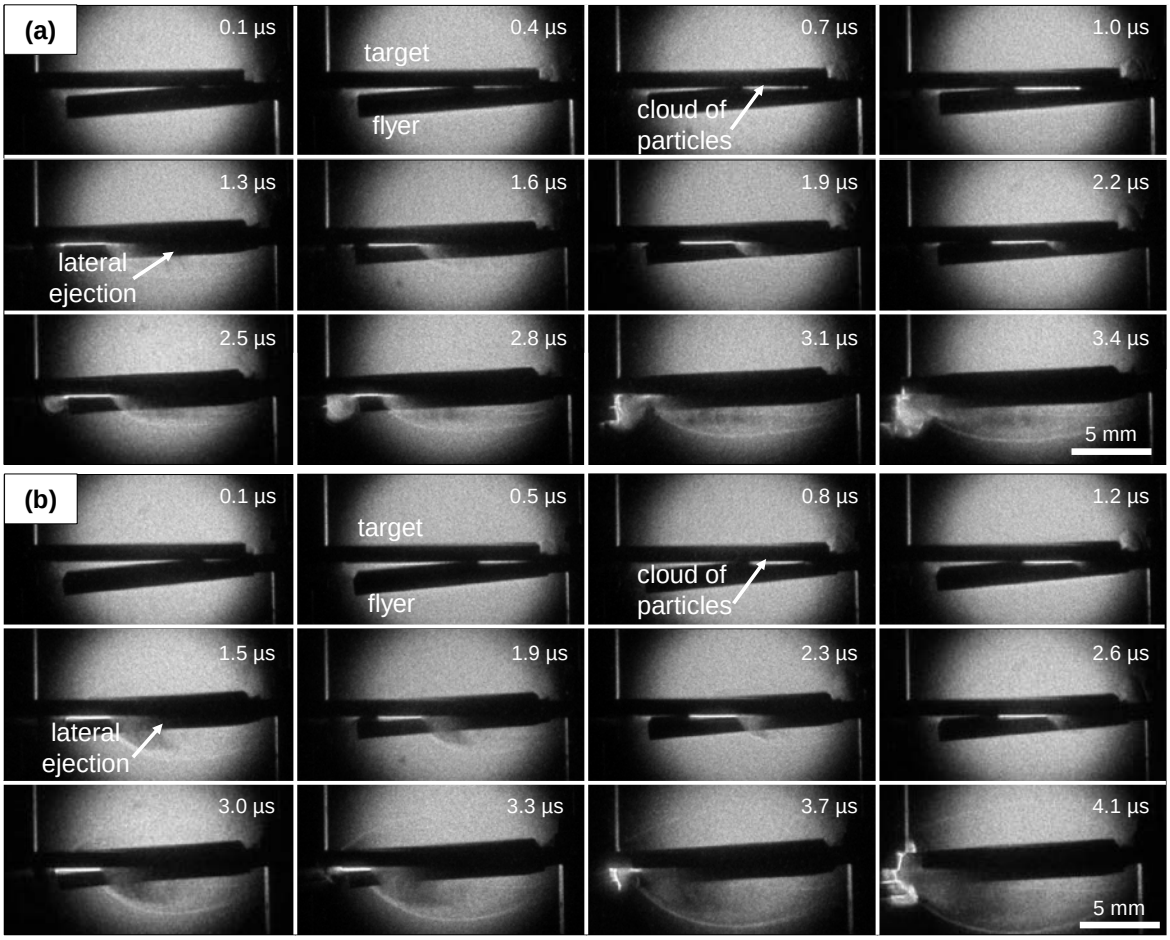

Figure 6: High Speed Imaging studies captured by the ML at the lower collision angle boundary at v_{imp} = 262 m/s. Each study consisted of three experiments taken at different delays. At β = 3.7° no weld was achieved (a), at β = 5°the samples were welded (b). The amount of CoP increased during the collision process, and it partly left the joining gap laterally (arrows). The bright glowing indicated a high temperature of the CoP.

No glare from the CoP was detected at the higher collision angle boundary, indicating that its temperature is lower due to lower compression in the joining gap. But in both series a separation of the CoP from the apex of the joining gap is visible, see Fig. 7. While this separation occurred comparatively at the beginning of the collision process for the non-welded series (b), it did not occur until the last third for the welded series (a). Furthermore, the amount of CoP in the joining gap was larger for series (a), where it grew with the progression of the collision. From the separation, it can be concluded that the responsible mechanism for the formation of the CoP, e.g., the jet, was either not formed for the non-welded series (b) or its formation was stopped (a). In the case of series (b), several particles were spalled from the surfaces during initial contact of the samples, but the collision conditions were not suitable to start jet or bond formation. In contrast, for series (a) the CoP grew continuously during the collision process. But the location of the first visible separation corresponds with the typical weld interface at large collision angles, which was shown for a

Figure 7: High Speed Imaging studies captured by the ML at the upper collision angle boundary at v_{imp} = 262 m/s. Each study consisted of three experiments taken at different delays. At β = 14.0° a weld was achieved (a), at β = 16.2° the samples were not welded (b). The accumulation of the CoP during the collision was higher in series (a) than in (b). A separation of the CoP from the apex of the joining gap starts earlier at (b) than at (a).

similar collision angle (13.6°) in (Niessen und Groche 2019). At this weld interface type, the bond formation stopped abruptly after two thirds of the sample length. A metallographic analysis of the weld interface in (Niessen et al. 2020) showed that jet formation stopped at this transition point. This was explained with the limited amount of energy input which was not sufficient to sustain the bending process for closing the joining gap and the formation of the jet by plastic deformation of the jet (Groche et al. 2019). At smaller collision angles, the heat stored in the CoP, might enhance the plastic deformation due to the lowered local flow stress at the surfaces (Niessen et al. 2020). Contrastingly, this effect is negligible at larger collision angles because the CoP was heated less and had a larger volume to spread in the gap.

4 Summary

In this study the collision welding process was investigated using an image intensifier camera on a mechanically driven model test rig. The results confirm recent findings on the important role of the CoP for bond formation. The following conclusions can be drawn:

- The bright glow of the CoP at small collision angles could be related to the higher compression in the joining gap. This explains the increased occurrence of melting at small collision angles in former research.
- The high-speed images showed that smaller collision angles prevent the ejection of the glowing CoP and confirmed its influence on bond formation either by causing excessive melting due to the stored heat or the inhibited contact of the base material.
- At larger collision angles, a separation of the CoP from apex of the joining gap was found and related to the prevented surface activation by the jet from former research which corresponds with the spatial weld interface formation.
- The determined accumulation of the CoP during the collision process indicates an unsteadiness at otherwise constant process parameters. How this affects local bond formation has to be examined in future.

5 Acknowledgement

The presented results have been generated within the research project “investigation of the formation mechanisms of the bonding zone in collision welding” (GR 1818/49-3) as part of the priority program 1640 “joining by plastic deformation” that was kindly funded by the German research foundation (DFG). As well, we would like to thank Mr. Walter Tutsch of PCO AG for the support during the implementation of the image intensifier camera set up.

References

Bellmann, Joerg; Lueg-Althoff, Joern; Schulze, Sebastian; Hahn, Marlon; Gies, Soeren; Beyer, Eckhard; Tekkaya, A. (2019): Thermal Effects in Dissimilar Magnetic Pulse Welding. In: *Metals* 9 (3), S. 348. DOI: 10.3390/met9030348.

Bellmann, Jörg; Lueg-Althoff, Jörn; Niessen, Benedikt; Böhme, Marcus; Schumacher, Eugen; Beyer, Eckhard et al. (2020): Particle Ejection by Jetting and Related Effects in Impact Welding Processes. In: *Metals* 10 (8), S. 1108. DOI: 10.3390/met10081108.

Carpenter, S. H.; Wittman, R. H. (1975): Explosion Welding. In: *Annu. Rev. Mater. Sci.* 5 (1), S. 177–199. DOI: 10.1146/annurev.ms.05.080175.001141.

Cowan, George R.; Holtzman, Arnold H. (1963): Flow Configurations in Colliding Plates: Explosive Bonding. In: *Journal of Applied Physics* 34 (4), S. 928–939. DOI: 10.1063/1.1729565.

Deribas, A. A.; Zakharenko, I. D. (1974): Surface effects with oblique collisions between metallic plates. In: *Combust Explos Shock Waves* 10 (3), S. 358–367. DOI: 10.1007/BF01463767.

Groche, P.; Becker, M.; Pabst, C. (2017): Process window acquisition for impact welding processes. In: *Materials & Design* 118, S. 286–293. DOI: 10.1016/j.matdes.2017.01.013.

Groche, Peter; Niessen, Benedikt; Pabst, Christian (2019): Process boundaries of collision welding at low energies. In: *Materialwiss. Werkstofftech.* 50 (8), S. 940–948. DOI: 10.1002/mawe.201900027.

Ishutkin, S.; I. Kirko, V.; A. Simonov, V. (1980): Thermal action of shock-compressed gas on the surface of colliding plates. In: *Combustion Explosion and Shock Waves - COMBUST EXPL SHOCK WAVES-ENGL* 16, S. 663–667. DOI: 10.1007/BF00741515.

Lysak, V. I.; Kuzmin, S. V. (2003): Explosive welding of metal layered composite materials. Kiev: E. O. Paton Electric Welding Institute (Welding and allied processes).

Mori, Akihisa; Tanaka, Shigeru; Hokamoto, Kazuyuki (2019): Observation for the High-Speed Oblique Collision of Metals. In: Explosion Shock Waves and High Strain Rate Phenomena, Bd. 13. Explosion Shock Waves and High Strain Rate Phenomena, 03/19-21/2019: Materials Research Forum LLC (Materials Research Proceedings), S. 74–78.

Niessen, Benedikt; Groche, Peter (2019): Weld interface characteristics of copper in collision welding. In: Lander Galdos (Hg.): Proceedings of the 22nd International ESAFORM Conference on Material Forming. ESAFORM 2019: 8-10 May 2019, Vitoria-Gasteiz, Spain. ESAFORM. AIP Publishing LLC (AIP Conference Proceedings, volume number 2113), S. 50018.

Niessen, Benedikt; Schumacher, Eugen; Lueg-Althoff, Jörn; Bellmann, Jörg; Böhme, Marcus; Böhm, Stefan et al. (2020): Interface Formation during Collision Welding of Aluminum. In: *Metals* 10 (9), S. 1202. DOI: 10.3390/met10091202.

Oertel, Herbert; Böhle, Martin (2010): Übungsbuch Strömungsmechanik. Grundlagen, Grundgleichungen, analytische und numerische Lösungsmethoden, Softwarebeispiele.

Pabst, Christian; Sharafiev, Semen; Groche, Peter; Wagner, Martin F.X. (2014): A Novel Method to Investigate the Principles of Impact Welding: Development and Enhancement of a Test Rig, Experimental and Numerical Results. In: *AMR* 966-967, S. 500–509. DOI: 10.4028/www.scientific.net/AMR.966-967.500.

Stern, A.; Shribman, V.; Ben-Artzy, A.; Aizenshtein, M. (2014): Interface Phenomena and Bonding Mechanism in Magnetic Pulse Welding. In: *J. of Materi Eng and Perform* 23 (10), S. 3449–3458. DOI: 10.1007/s11665-014-1143-0.

Wang, Huimin; Wang, Yuliang (2019): High-Velocity Impact Welding Process: A Review. In: *Metals* 9 (2), S. 144. DOI: 10.3390/met9020144.